American Mineralogist, Volume 88, pages 2007–2015, 2003

The structure of disordered mackinawite

MARIËTTE WOLTHERS,[1,*] SJIERK J. VAN DER GAAST,[2] AND DAVID RICKARD[3]

[1]Department of Geochemistry, Faculty of Earth Sciences, Utrecht University, Utrecht, The Netherlands
[2]Royal Netherlands Institute for Sea Research (NIOZ), Texel, The Netherlands
[3]School of Earth, Ocean, and Planetary Sciences, Cardiff University, Cardiff, Wales, U.K.

ABSTRACT

Synthetic Fe^{2+} monosulfide, FeS_{am}, displays a disordered tetragonal mackinawite structure. It is nanocrystalline, with an average primary particle size equivalent to a crystallite size of 4 nm and a corresponding specific surface area of 350 m^2/g. It can be described in terms of a mixture of two end-member phases with different long-range ordering, which we refer to as MkA and MkB. MkA has an average primary particle size of 2.2×1.7 nm and lattice parameters $a = b = 4.0$ Å, $c = 6.6 \pm 0.1$ Å. MkB has an average primary particle size of 7.4×2.9 nm and lattice parameters $a = b = 3.7$ Å, $c = 5.5 \pm 0.2$ Å. A typical disordered mackinawite precipitate consist of 30% MkA and 70% MkB and the proportion of MkA decreases with age. Lattice expansions relative to crystalline mackinawite ($a = b = 3.7$ Å, $c = 5.0$ Å) may be explained by intercalation of water molecules between the tetrahedral sheets and by lattice relaxation due to small crystallite size.

The formation of two phases of FeS_{am} is consistent with competing pathways involved in its formation from aqueous solution. MkA may be equivalent to sheet-like precipitated aqueous FeS clusters. The reactivity of FeS_{am} is dependent on the proportion of the two end-member phases. These in turn are dependent on the conditions of formation, especially pH, and the age of the precipitate. These observations partly explain the reported differences in FeS_{am} reactivity in experimentation and in the environment. The structural model has implications for the behavior of natural acid volatile sulfides in scavenging elements from solution in natural environments.

INTRODUCTION

Disordered mackinawite is a highly reactive phase with a high adsorptive capacity for divalent metals (e.g., Kornicker 1988; Morse and Arakaki 1993; Arakaki and Morse 1993; Wharton et al. 2000). It is typically the first iron sulfide to form in aqueous environments and with time it may react to form more stable iron sulfide phases such as ordered mackinawite, greigite, and ultimately pyrite or pyrrhotite (e.g., Rickard et al. 1995; Hurtgen et al. 1999). Mackinawite possesses a tetragonal layer structure (Fig. 1), where the Fe atoms are linked in a tetrahedral coordination to four equidistant sulfur atoms. The Fe atoms form sheets with Fe in perfect square planar coordination and with an Fe-Fe distance of 2.5967 Å (Lennie et al. 1995), which is similar to the Fe-Fe distance in α-iron and underlines the importance of Fe-Fe bonding in the material. These Fe sheets are stacked along the **c** axis, with Van der Waals forces between S atoms holding the sheets together (Vaughan and Craig 1978). Non-stoichiometry is observed in natural mackinawite and appears to result from sulfur deficiency (Taylor and Finger 1970). In synthetic mackinawite, sulfur excess is commonly observed (e.g., Rickard 1968; Berner 1974). However, in a Rietveld analysis of the structure of synthetic mackinawite, Lennie et al. (1995) were unable to detect any crystallographic evidence for vacancy occupancy or surplus Fe occupancy. They found that the FeS_4 tetrahedra are almost perfectly regular, with a much smaller degree of distortion than had been previously reported, and concluded that a satisfactory structural refinement may be achieved by assuming stoichiometric tetragonal FeS.

The bulk properties of synthetic disordered mackinawite have been described by several authors. There are broadly three ways of synthesizing mackinawite at low temperature: by the reaction of aqueous sulfide solutions with either (1) metallic iron or (2) ferrous iron (Berner 1964; Rickard 1969; Lennie and Vaughan 1996), or (3) via sulfate-reducing bacteria (Rickard 1968; Watson et al. 2000). The reaction of metallic iron with aqueous sulfide results in a more crystalline mackinawite than reactions (2) and (3) (Lennie and Vaughan 1996; Mullet et al. 2002). With the notable exception of Watson et al. (2000), all recent studies aiming to describe the properties of bulk disordered mackinawite studied the more crystalline solid (Lennie and Vaughan 1996; Mullet et al. 2002). However, the reaction of Fe^{2+} with inorganic and bacterial aqueous sulfide produces disordered mackinawite, which is very similar to natural disordered mackinawite (Berner 1967; Spadini et al. 2003).

In this paper, disordered mackinawite is defined as the first precipitated Fe^{2+} monosulfide phase formed through the reaction between aqueous Fe^{2+} or metallic iron and S^{-2} under ambient conditions. Lennie and Vaughan (1996) showed that this phase, which is sometimes referred to as "amorphous FeS," displays long-range mackinawite ordering. This phase is re-

* E-mail: wolthers@geo.uu.nl

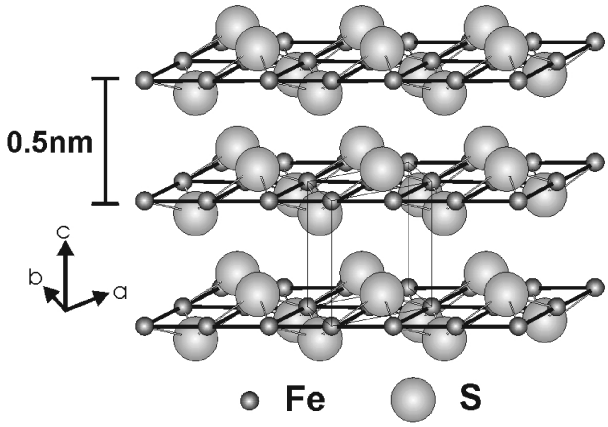

FIGURE 1. Sketch of the mackinawite structure viewed from ca. 30° above the (001) plane. The tetragonal unit cell is indicated. The Fe-Fe bond length is 2.60 Å, which is extremely close to that of α-iron and suggests significant Fe-Fe bonding. The Fe atoms are in square planar coordination and constitute the (001) plane of the structure. The sheets of Fe atoms are separated by ca. 0.5 nm and the sheets are weakly held by Van der Waals bonding between the S atoms. The interstices between the sheets are potential sites for other molecules such as H_2O. This stick-and-ball representation uses conventional ionic radii for clarity. The Fe-Fe bonding, the Fe-S covalent, and S-S Van der Waals bonding make substantial changes to the effective atomic radii.

ferred to as FeS_{am} in the present paper.

Rickard (1995) showed that the rate of precipitation is fast and can be described in terms of an Eigen-Wilkins mechanisms with two competing mechanisms resulting from the pH dependence of aqueous sulfide speciation:

$$Fe^{2+} + H_2S \rightarrow FeS_{am} + 2H^+ \quad (1)$$

$$Fe^{2+} + 2HS^- \rightarrow Fe(HS)_2 \rightarrow FeS_{am} + H_2S \quad (2)$$

where reaction 1 is dominant at pH < 7 and 2 is dominant at pH > 7.

The objective of this study is to develop a model for the structural properties of the disordered mackinawite produced by reacting aqueous Fe^{2+} with aqueous S^{-2}. Low-angle X-ray powder diffraction (LAXRPD) analyses were used to measure the average diameter of the primary particles of freeze-dried FeS_{am} and to compare these results with transmission electron microscopy (TEM) results and specific surface area measurements from freeze-dried FeS_{am}. Furthermore, from conventional X-ray powder diffraction (XRPD) data the size of the crystalline domains (i.e., portions of the structure that diffract X-rays coherently) was estimated for freeze-dried and suspended FeS_{am}.

MATERIALS AND METHODS

Chemicals

All chemicals were of analytical grade and were used without further purification; solutions were prepared from Milli-Q water and purged for at least 30 minutes with purified O_2-free N_2 gas before use. N_2 was purified by bubbling through a succession of two 15 wt% pyrogallol in 50 wt% KOH solutions to remove O_2, a Chrompack dioxygen and sulfide scrubber for additional cleaning, and Milli-Q water to saturate the N_2 with water. Solutions of S^{-2} and Fe^{2+} were prepared before every experiment by dissolving $Na_2S{\cdot}9H_2O$ (Fisher Chemicals) and Mohr's salt [$Fe(NH_4)_2(SO_4)_2{\cdot}4H_2O$; Merck], which is relatively resistant to oxidation, in either purged Milli-Q water or background electrolyte of varying KNO_3 (Fisher Chemicals) concentration. Syntheses were run under O_2-free conditions by directly flushing the reaction vessel with purified N_2. The O_2 concentration in the reaction vessels was below 0.03 ppm, which is <1 μ*M*, which is the detection limit of the Orion oxygen probe 850 used to measure O_2 in solution.

Materials

Disordered mackinawite was synthesized in two ways: (1) FeS_{am} was prepared in advance and freeze-dried. This material was used for the bulk solid characterization and determination of the specific surface area by the N_2-BET adsorption method. Freeze-dried FeS_{am} was prepared less than a week in advance by mixing 100 mL Mohr's salt solution (0.6 *M*) with 100 mL sulfide solution (0.6 *M* $Na_2S{\cdot}9H_2O$) under N_2, filtrating the suspension through a Whatman No.1 filter (pore size 11 μm), and freeze drying the product for 3 to 4 days. Effectively, the freeze-dried FeS_{am} has aged for less than half an hour. The conclusion that freeze-drying essentially froze the FeS_{am} in time was demonstrated by the observation that replacing the freeze-dried material in aqueous solution resulted in the continuous crystallographic development of material similar to that observed in the suspended material. After freeze-drying, the FeS_{am} was stored under N_2 atmosphere at –18 °C upon use. (2) Suspended FeS_{am} was precipitated in situ for XRPD measurements by adding a 40 m*M* Mohr's salt solution to a 40 m*M* disodium sulfide solution while constantly flushing with dinitrogen; flocculated FeS_{am} formed rapidly and was left to age for varying times prior to analysis.

Solid characterizations

TEM images, selected-area electron diffraction patterns (SAED), and energy-dispersive X-ray (EDX) analyses of freeze-dried FeS_{am} were collected with a Philips CM200 FEG-TEM (200 kV). Approximately 0.5 mg of freeze-dried FeS_{am} dispersed in acetone was quickly loaded in air onto a copper grid with a thin biofilm, carbon coated, and loaded into a low-background specimen microscope holder. SAED patterns and TEM images were recorded photographically. Since the particles may be smaller than the interaction volume of the 200 kV electron beam and since no calibration could be done, the EDX data were used qualitatively.

XRPD was carried out using a self built θ-θ goniometer equipped with a long-fine-focus X-ray tube (Cu*K*α radiation, 40 kV, 40 mA), variable divergence and anti-scatter slits, and a Kevex solid-state Si(Li) detector. Approximately 0.5 g of freeze-dried FeS_{am} was loaded under a nitrogen atmosphere within a glove bag into a 1 mm deep depression in a metal support and then the surface of the material was carefully leveled with the top of the specimen holder using light pressure from a glass slide. The specimen was placed in an environmental chamber with Mylar windows, which was mounted on the goniometer. The chamber was constantly flushed with dry N_2 to prevent oxidation of the specimen. A series of 12 XRPD patterns, in the range of 1–60° 2θ, were collected using the following settings: 20 mm irradiated specimen length, 0.3 mm receiving slit, 3 s/0.05° 2θ counting time. The 2θ range chosen facilitates the determination of both primary particle size, through diffraction by stacked particles with LAXRPD, and lattice *d*-spacing and crystalline domain size, through conventional XRPD. Afterward, the XRPD patterns were carefully checked for temporal variability due to oxidation or aging during analysis. No significant differences between the 12 patterns were found and therefore they could be summed to give one pattern over the 1–60° 2θ range with a net counting time of 36 s per step of 0.05° 2θ. The detection limit of a phase is estimated to be ~1%.

The XRPD patterns were corrected for the Lorentz-polarization factor (McEwan et al. 1961) and for the diffracting specimen volume. Peak positions and widths were obtained by fitting Pearson-IV-functions (PEAKFIT 4.0, Jandell). The average diameter of the primary particles of the disordered mackinawite was obtained by either multiplying the LAXRPD peak position by a factor of 1.225 based on the approximation that the particles are hexagonally close-packed or by assuming the particles to be regularly stacked platy particles, that is, no correction factor. The assumption that the particles are stacked plates is supported by the observation by TEM of diffraction fringes along the edges of the particles. The primary particle diameter was taken as the average of the two obtained values.

Additionally, XRPD patterns were collected from a thick (settled and decanted) FeS_{am} suspension quickly loaded in air onto a low background sample holder (silicon wafer), and covered with a 2.5 μm thick Mylar foil. A series of

XRPD patterns, in the range of 9–24° 2θ, were collected from the suspended FeS_{am} using the following settings: 20 mm irradiated specimen length, 0.4 mm receiving slit, 1° antiscatter slit, 30 s/0.1° 2θ counting time. Blank patterns of a thick calcite suspension loaded on the low background holder were collected with the same settings, and subtracted from the FeS_{am} patterns to correct for the interference from water. A conservative estimate of the detection limit is ~5%.

The average diameters of the crystalline domains were determined from the conventional XRPD patterns by applying the Scherrer equation:

$$L = K\lambda(\beta \cos \theta)^{-1} \quad (3)$$

to the (001) peak, where L is the average diameter of the domain, K is the factor 0.91 (Brindley 1980), λ is the wavelength of the applied X-rays (0.154 nm for Cu$K\alpha$), β is the full width (in radians) at half maximum (FWHM) of the peak, and θ is the angle of the position of the peak.

The specific surface area (SSA) of freeze-dried FeS_{am} was determined in triplicate following the N_2-BET adsorption method, using a Micromeritics Tristar 3000 instrument. Approximately 400 mg samples were loaded into the appropriate sample holder, dried for 12 hours at 60 °C under gently flowing N_2 and evacuated via the Tristar 3000. The free surface area was measured with He gas prior to N_2-BET adsorption. Micromeritics kaolinite with a specific surface area of 16.2 ± 0.8 m^2/g was used as a reference standard. To compare the measured specific surface area to the bulk solid characterizations, the particle size was estimated from the measured SSA assuming a spherical particle shape and a density of 4.1 g/cm^3.

RESULTS

The initial examination of freeze-dried FeS_{am} was performed using TEM (Fig. 2). The FeS_{am} occurs as micrometer-sized aggregates consisting of smaller subparticles. This aggregation resulted from filtration and subsequent freeze-drying of an FeS_{am} suspension. The subparticle sizes fall roughly into a range of 20–400 nm diameter, although it was difficult to clearly identify individual subparticles within the aggregates. Calculating the specific surface area based on the minimum particle size yields ~73 m^2/g and based on the maximum particle size yields ~4 m^2/g (Table 1). EDX measurements were made on several individual FeS_{am} aggregates and yielded an approximate Fe:S ratio of 1, indicating a mackinawite-like composition. No other phases were observed in the TEM analyses. The FeS_{am} aggregates showed weak rings in SAED (Fig. 2b), confirming the disordered character of FeS_{am}.

In the conventional XRPD pattern from freeze-dried FeS_{am} (Fig. 3a, spectrum at an angle >10° 2θ) the broad peaks are indicative of a disordered phase, with peak intensities and positions in reasonable agreement with previously reported data for mackinawite (Kuovo et al. 1963; Rickard 1969). At approximately 42° 2θ, there is a small contribution from the brass specimen holder. The best fit (R^2 = 0.994) to the diffraction pattern was found with a minimum of two peak sets and is given as the smooth curve displayed below the experimental data in Figure 3a. The relevant individual peaks of the fit are also shown in Figure 3a and the crystallographic data extracted from this fit, assuming the conventional tetragonal unit cell for mackinawite, are listed in Table 2. The 50° 2θ peak is rather complex and its fit is omitted from the discussion. However, even though the sensitivity of the fit of this peak is low, and the peak assignment is obscure, for the sake of completeness the crystallographic data for the *hkl* reflections in this part of the pattern are

TABLE 1. Particle size and SSA values for freeze-dried FeS_{am}

Method	SSA (m^2/g)	Diameter (nm)	Reference
TEM	*4–73*	20–400	(1)
BET	47 ± 1	*31*	(1)
LAXRPD	*350*	4.2 ± 0.5	(1)
BET	80	*18*	(2)
BET	16–21	*70–90*	(3)
XRPD + SEM	*40–140*	10–35	(4)
BET	36.5	*40*	(4)
BET	53.0 ± 46.3	*28 (15–220)*	(5)
BET	7	*210*	(6)
Microscopy	*44*	33	(7)

Notes: Values were measured and calculated (using a density of 4.1 g/cm^3; approximate values, given in italic) from: (1) this study, (2) Widler and Seward (2002), (3) Benning et al (2000), (4) Rickard (1997), (5) Kornicker (1988), (6) Taylor et al. (1979), (7) Rickard (1975). SEM = scanning electron microscopy. TEM = transmission electron microscopy; BET = gas adsorption method; LAXRPD = low-angle X-ray powder diffraction; SEM = scanning electron microscopy.

TABLE 2. Conventional XRPD data for disordered mackinawite from freeze-dried FeS_{am} MkA and MkB (see text) compared with crystalline reference mackinawite (Lennie et al. 1995)

	Reference Mk		Freeze-dried MkA		Freeze-dried MkB	
hkl	*d* (Å)	*I* (%)	*d* (Å)	*I* (%)	*d* (Å)	*I* (%)
001	5.0328	100	6.60	100	5.48	100
101	2.9672	50	3.33	51	3.36	41
110	2.5976	8	2.84	27	2.58	7
111	2.3082	70	2.42	41	2.30	47
200	1.8368	38	2.00	35	1.95	10
112	1.8074	82	1.88	52	1.83	29
201	1.7254	29	1.77	50	1.73	23
003	1.6776	9	1.84	44	1.81	30
211	1.5617	12	1.63	21	1.57	12

Note: The relative intensities (*I*) are in % peak surface area of the (001) signal.

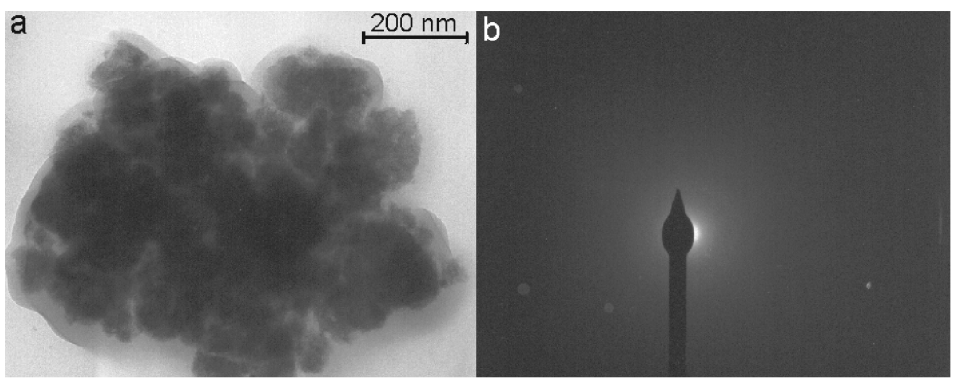

FIGURE 2. TEM image of freeze-dried FeS_{am} (scale bar is 200 nm). The diffraction fringes observed around the edges of the mackinawite particles (**a**) suggest that aggregates consist of stacked, thin plate-like mackinawite crystals, which is consistent with the known structure of the mineral and with the electron powder diffraction image obtained from these aggregates (**b**).

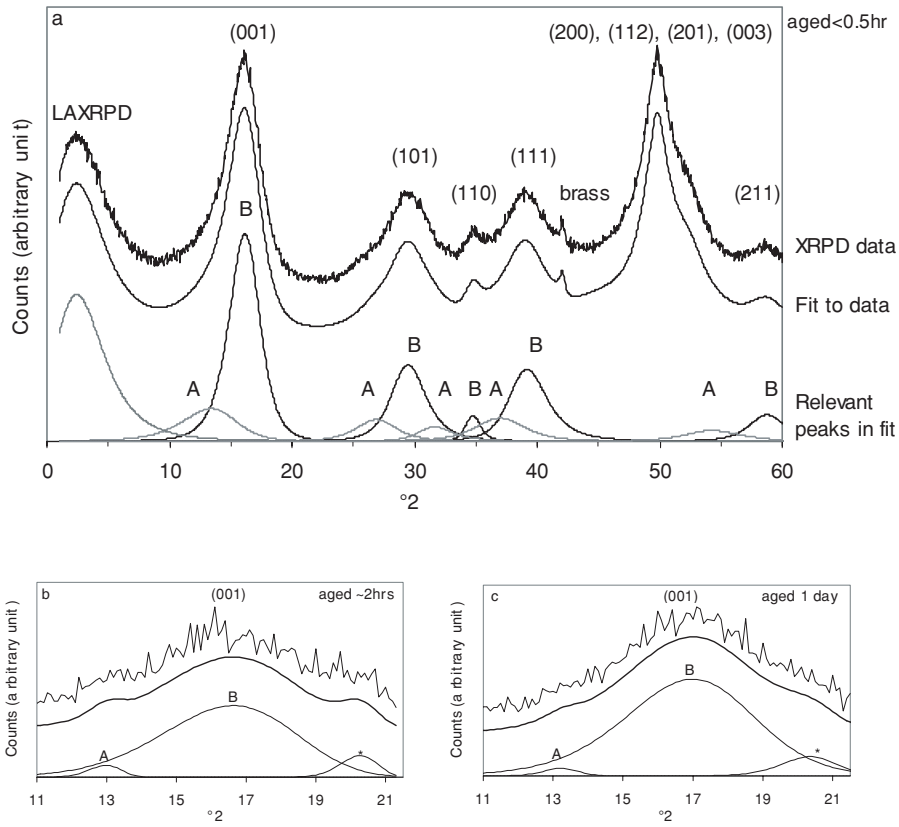

FIGURE 3. Conventional and LAXRPD pattern and the corresponding fit ($R^2 = 0.994$) for freeze-dried FeS_{am} (**a**). XRPD patterns and fits for a freshly prepared suspended FeS_{am} which has aged for ~2 h (**b**) and 1 day (**c**), with respectively $R^2 = 0.93$ and $R^2 = 0.95$. Crystallographic data derived from the fits are listed in Tables 2 to 4. A and B in the spectra correspond to FeS_{am} phases MkA and MkB respectively (see text). * in (**b**) and (**c**) is introduced by the (102) calcite *d*-spacing (see text).

listed in Table 2. Note that the shape of the 50° peak, including its shoulder at high angle, can only be explained by a combination of peaks from mackinawite spacings.

The low-angle XRPD pattern (Fig. 3a, <~10° 2θ) shows a distinct maximum between 1–8° 2θ for freeze-dried FeS_{am}. Comparable low-angle reflections were found for different clay particles (Van der Gaast et al. 1985, 1986) and for ferrihydrite particles (Parfitt et al. 1992). The low-angle peak position indicates the average primary particle size. In our pattern, the tail of the peak toward higher angles is caused by a poor stacking of the particles and/or the grain size distribution. If the FeS_{am} particles are assumed to be hexagonally close-packed spheres, then the LAXRD maximum indicates an average diameter of 4.6 nm (correction factor 1.225). If the FeS_{am} particles are assumed to be regularly stacked platy particles, then the maximum indicates an average diameter of 3.7 nm (no correction factor). Thus, on average, the primary particle size will be 4.2 ± 0.5 nm. Estimation of the specific surface area based on this average primary particle size yields 350 ± 40 m^2/g (Table 1).

The diffraction patterns collected from in situ prepared suspended FeS_{am} (Figs. 3b and 3c) show a similar broad (001) peak for precipitated FeS_{am} around 15° 2θ as for freeze-dried FeS_{am} (Fig. 3a). In Figure 3b, the diffraction pattern is shown for suspended FeS_{am}, which has been aged for ~2 hours; the diffraction pattern depicted in Figure 3c is from 1 day old suspended FeS_{am}. The low signal-to-background ratio permitted the measurement of the most intense (001) peak only. The diffraction patterns were fitted graphically and the best fit (R^2 = 0.93 for Fig. 3b and $R^2 = 0.95$ for Fig. 3c) is given as a smooth curve below the raw patterns together with the individual peaks of the fit. Based on the fit of the freeze-dried FeS_{am} (Fig. 3a), the suspended-FeS_{am} patterns were fitted with two peaks as well. The relative contribution of low-amplitude peaks to the total diffracted signal is less in Figures 3b and 3c than in Figure 3a. The third peak in Figures 3b and 3c is an artificial one, introduced by (102) *d*-spacing of calcite at 23.01° 2θ from the blank pattern after correction. The crystallographic data extracted from these fits are listed in Table 3.

The XRPD patterns collected from the freeze-dried FeS_{am} (Fig. 3a) and from the suspended FeS_{am} (Figs. 3b and 3c) could be fitted with a minimum of two peak sets, because of a tailing of peaks toward low angles. Such a tail was also found in patterns of freeze-dried FeS_{am} from other batches, in patterns collected at different instrument settings, and in patterns from both freeze-dried and suspended FeS_{am}. The fact that the patterns could be fitted with a minimum of two peak sets indicates that the material is a mixture of at least two disordered mackinawite phases, referred to as MkA and MkB, with varying *d*-spacing and crystallinity. The low-amplitude peak set of the freeze-dried material (Fig. 3a) represents the *d*-spacings for MkA; the high-amplitude peak set in Figure 3a represents the *d*-spacings for MkB. The relative proportions of MkA and MkB vary with age (Table 3). The unit-cell parameters derived from the XRPD patterns are listed in Table 4.

The average dimensions of the crystalline domains were determined from the FWHM values of the (001) and (110) peaks

TABLE 3. X-ray data for disordered mackinawite from the XRPD analyses of suspended FeS_{am} MkA and MkB (see text) compared with freeze-dried FeS_{am}

	MkA		MkB	
	(001) *d* (Å)	*I* (%)	(001) *d* (Å)	*I* (%)
Freeze-dried FeS_{am}, <0.5 h	6.60	22	5.48	78
Suspended FeS_{am}, ~2 h	6.8	4	5.3	96
Suspended FeS_{am}, 1 day	6.7	2	5.2	98

Note: The relative intensities are in % peak surface area of the (001) signal.

TABLE 4. Lattice parameters for disordered mackinawite

	a = *b* (Å)	*c* (Å)	Reference
Freeze-dried MkA (<0.5 h)	4.02	6.60	(1)
Suspended MkA (~2 h)	n.d.	6.8	(1)
Suspended MkA (~1 day)	n.d.	6.7	(1)
Freeze-dried MkB (<0.5 h)	3.65	5.48	(1)
Suspended MkB (~2 h)	n.d.	5.3	(1)
Suspended MkB (~1 day)	n.d.	5.2	(1)
Freeze-dried	3.67	5.05	(2)
Vacuum-dried	3.67	5.03	(3)
Suspended	3.68	5.03	(4)
Synthetic crystalline	3.6735(4)	5.0328(7)	(5)

Notes: (1) this study, (2) Mullet et al. (2002), (3) Lennie and Vaughan (1996), (4) Rickard (1969), (5) Lennie et al. (1995). n.d. = not determined.

by applying the Scherrer equation (Eq. 3). From the pattern of the freeze-dried MkA phase (Fig. 3a), the calculated domain size is 2.2 nm along the **a** and **b** crystallographic axes and 1.7 nm along the **c** axis (that is, 5 by 5 by 3 unit cells in one MkA domain; Fig. 4a). For the MkB phase (Fig. 3a), the domain sizes is 7.4 nm along the **a** and **b** axes and 2.9 nm along the **c** axis (i.e., 20 by 20 by 5 unit cells in one MkB domain; Fig. 4b). For suspended MkA and MkB, only the domain dimensions along the **c** axis could be established, since only the (001) peak was measured (Figs. 3b and c). Due to the low signal-to-background ratio, the FWHM values are not as accurate as for those from the freeze-dried material. The domain size here is ~2 nm for MkA and ~3 nm for MkB.

Precision of the XRPD patterns

To check the samples for oxidation, the XRPD patterns were inspected for the presence of possible oxidation products of FeS_{am}: pyrite, greigite, elemental sulfur, magnetite, and goethite (Benning et al. 2000; Boursiquot et al. 2001). The major diffraction peaks of pyrite (JCPDS 06-0710) at 33.04 and 56.28° 2θ are absent in the patterns and, therefore, the presence of pyrite can be excluded. Similarly, no evidence was found for other products of enhanced FeS_{am} oxidation since the major diffraction peaks of elemental sulfur (JCPDS 08-0247) at 23.09° 2θ, magnetite (Cornell and Schwertmann 1996) at 43.035° 2θ, and goethite (JCPDS 29-0713) at 21.24° 2θ are absent in the patterns. While most major diffraction peaks of greigite (JCPDS 16-0713) overlap with those of mackinawite, the diffraction of a 30% relative intensity peak at 25.43° 2θ, which is in an area of low total diffraction intensity, is not detectable. In short, the XRPD patterns do not show any diffraction by phases formed during weak or enhanced oxidation of FeS_{am}. Therefore, it can be concluded that the XRPD patterns represent only pristine disordered mackinawite.

The occurrence of the low-angle tail is consistent throughout the XRPD patterns. The XRPD patterns differ in this low-angle tailing from patterns collected from more crystalline mackinawite samples (e.g., Benning et al. 2000; Mullet et al. 2002). This difference can be explained by the structural evolution of FeS_{am} as discussed below. With time, the relative contribution of the least-ordered phase, MkA, decreases with respect to the contribution of MkB and, hence, the low-angle tailing of the diffraction peaks decreases.

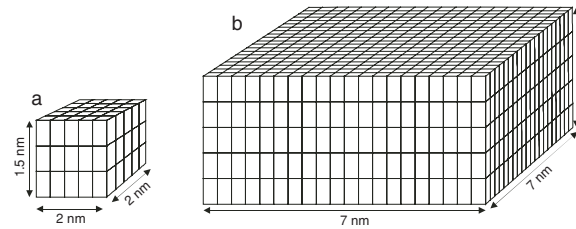

FIGURE 4. Models for the crystalline domains in disordered mackinawite as discussed in text. (**a**) one crystalline MkA domain, consisting of 75 unit cells, and (**b**) one crystalline MkB domain, consisting of 2000 unit cells. The size of the unit cell is the same for MkA and MkB in this sketch, actual values of the unit cells are listed in Table 4.

DISCUSSION

Primary particle size and specific surface area

The primary particle sizes and corresponding specific surface areas (SSA) listed in Table 1, show a large variance. The particle-size range from the TEM imaging is broad owing to the difficulty to distinguish individual particles in the strongly aggregated freeze-dried material. The lower end of the size range is comparable with the particle size calculated from the BET-measured specific surface area (47 ± 1 m^2/g) and with most other reported or calculated diameters. A much smaller size, 4.2 ± 0.5 nm, yielding a SSA of 350 ± 40 m^2/g, was measured by LAXRPD.

This broad range of particle sizes and specific surface area measurements has been determined for, or calculated from, properties of dried and therefore strongly aggregated, disordered mackinawite. Kornicker (1988) reported a 53.0 ± 46.3 m^2/g BET surface area for disordered mackinawite and explained the large standard deviation by drying artifacts. Watson et al. (2000) described similar effects of freeze-drying on an iron sulfide mixture, consisting of disordered greigite and mackinawite, formed by sulfate-reducing bacteria. Preliminary neutron scattering data showed the presence of 2 nm nanoparticles or holes. Watson et al. (2000) found a BET specific surface area of 18.4 m^2/g while magnetic properties, neutron scattering, and the adsorption isotherms of several heavy metals indicated a specific surface area on the order of 400–500 m^2/g. In fact, the interpretation of this material as nanoparticles rather than holes might better explain the difference between the surface areas suggested by the measurements of trapped magnetic flux and the BET measurements. In the present study, freeze-dried, pure disordered mackinawite ap-

pears to behave similarly leading to a marked divergence between the measured BET surface area and the calculated surface area from the XRPD data.

Compared to the nanoparticulate iron sulfide mixture from Watson et al. (2000) and other fine-grained amorphous materials, the SSA estimated from the LAXRPD analyses seems the most realistic. Hydrous ferric oxide, for example, reportedly has an SSA ranging from 159–720 m^2/g (see Dzombak and Morel 1990) and amorphous silica 100–200 m^2/g (Dixit and Van Cappellen 2002). It is therefore proposed that disordered mackinawite has a specific surface area on the order of 350 m^2/g and a corresponding average primary particle size of ~4 nm. This is consistent with the suggestion of Rickard and Luther (1997) that a continuum of FeS sizes down to electroactive aqueous FeS clusters less than 5 nm in size exists. Thus, disordered mackinawite particles are nanoparticles, possibly nanocrystals, according to the definition of Waychunas (2001).

Crystal structural properties

The XRPD patterns for freeze-dried and suspended FeS_{am} show that the material is a mixture of at least two phases of different crystallinity (Fig. 3, Tables 2 and 3). The pattern for freeze-dried FeS_{am} is dominated by the more crystalline phase, MkB, forming ~78% of the (001) peak. The domain size for MkB extends over 2000 unit cells (Fig. 4b). If the crystalline domain is assumed to be spherical, its average diameter is 6.4 nm. Approximately 22% of the (001) peak for freeze-dried FeS_{am} consists of the less crystalline MkA. The MkA domain consists of 75 unit cells (Fig. 4a). Approximating the crystalline domain as spherical, its average diameter would be 2.0 nm. If the crystalline domains of MkA are also primary particles, analogous to MkB, then this particle size is equal to the average particle size of 2–3 nm Watson et al. (2000) found for their mackinawite-greigite mixture precipitated by SRBs. A mixture of 78% MkB with a (spherical) domain size of 6.4 nm and 22% MkA with 2.0 nm gives an average diameter of 5.4 nm, which is close to the average primary particle size established with LAXRPD. This suggests that each primary particle is one domain and thus a nanocrystal (Waychunas 2001). In suspended FeS_{am}, the domain size for MkA and MkB ranges from 2 to 3 nm respectively, which is comparable to the domains for freeze-dried disordered mackinawite.

It can be concluded that disordered mackinawite consists of at least two phases of different long-range ordering, the size of MkA domains being smaller to that of MkB domains. The simple two-phase model fits the pattern ($R^2 = 0.994$), and describes the crystal structure of disordered mackinawite. Precipitated FeS_{am} ripens within days to more crystalline mackinawite (Kornicker 1988). Ripening occurs either through aggregation and secondary growth or through Ostwald ripening. Our results suggest that the proportion of MkA decreases with aging (Table 3), consistent with this process.

Why can disordered mackinawite be represented by two end-member phases with differing crystallinities? One possibility is that the domain size distribution derives as a consequence of the "magic number" theory of cluster physics that suggests that certain numbers of molecules will have lower total energies and therefore form preferentially (e.g., Echt et al. 1982). We also note a coincidence between the competitive pathways for the formation of FeS from solution (Eqs. 1 and 2; Rickard 1995) and the two domain sizes observed in our work. Our experimental syntheses of disordered mackinawite were carried out between pH 6 and 8, where both H_2S and HS^- mechanisms for the formation of FeS occur. The presence of two competing pathways for FeS_{am} formation in aqueous solutions is consistent with the observation of two forms of FeS_{am} in this experimentation: for example, MkA being the precipitated clusters (Eq. 2) and MkB resulting from the more rapid direct precipitation route (Eq. 1).

Aqueous metal sulfide clusters have structures similar to the first formed metal sulfide precipitates (Luther et al. 1999, 2001). The structure and stoichiometry of the aqueous FeS clusters (Theberge and Luther 1997) have not been determined as yet. However, molecular models suggest that they should have structures similar to mackinawite and display a spectrum of molecular masses up to the formation of the first condensed phase. Aqueous FeS clusters are abundant in experimental (e.g., Theberge and Luther 1997) and natural systems (e.g., Rickard et al. 1999; Luther et al. 2001). Freeze-drying itself would act to increase the solution concentrations of the aqueous clusters through loss of water. The size of MkA, which consists of about 75 unit cells and therefore approximately 150 FeS molecules, is consistent with the suggestion that this material may represent the first condensed phase formed from the aqueous FeS clusters.

Lattice spacings

The lattice parameters for disordered mackinawite decrease with age and with drying (Table 4). Freeze-dried FeS_{am} is essentially the first precipitate, since it was filtered and dried immediately after precipitation, thus it was aged for less than half an hour. It showed all strong mackinawite reflections, in keeping with results from Lennie and Vaughan (1996) and Rickard (1969), indicating that the tetrahedral sheets form and start ordering (Fig. 1) within one hour after precipitation. Lattice parameters a and b of the freeze-dried MkB fraction are indistinguishable from crystalline mackinawite, although c is slightly larger. For the MkB fraction, c decreases with age toward the crystalline-mackinawite value (Table 4). Freeze-dried MkA has an expanded lattice along the three crystallographic axes relative to crystalline mackinawite. Lattice parameter c of the suspended MkA decreases with age and with freeze-drying. Apparently, the controlling factor of this lattice expansion is also influenced by the freeze-drying process.

Expansion along the **c** axis implies that the tetrahedral sheets lie further apart, while expansion along the **a** and **b** axes implies that the tetrahedra within the sheets are either dislocated or distorted relative to crystalline mackinawite (Fig. 1). In the past, expansions of the crystalline mackinawite lattice have been explained by excess cation uptake between sulfur-sulfur layers, in tetrahedral coordination with sulfur (Vaughan 1970). Additionally, Murowchick and Rickard (1997) explained (1) lattice expansions in young synthetic mackinawite, formed from alpha-iron corrosion, by repulsion between the adjacent S-Fe-S layers, and (2) different reflection intensity ratios by tetrahedral sheet offsets. In general, the MkA and MkB lattices can

expand relative to the crystalline standard for several reasons. For example, lattice relaxation through expansion or contraction with decreasing nanocrystallite size has been reported (see Waychunas 2001). Since disordered mackinawite is nanocrystalline, lattice expansion purely caused by small crystallite size affects the *a*, *b*, and *c* lattice parameters. MkA has a more expanded lattice (Table 5) and a smaller crystalline domain size, which may support lattice relaxation. Alternatively, lattice parameters can vary owing to lattice defects, substitutions, impurities, and hydration. Dang et al. (1998) performed a thorough study of several synthetic tetragonal hematite-like materials and they concluded that these hematites differ from pure bulk hematite in their precise lattice parameters due to incorporated structural water molecules or OH-groups with associated vacancies to balance charge. A similar scenario can be envisaged for disordered mackinawite. Based on Kornicker's (1988) finding that drying changes the physical properties of mackinawite, Morse et al. (1987) concluded that disordered mackinawite may be a hydrate. For example, within the structure of crystalline mackinawite water molecules can partly occupy the cavities enclosed by four tetrahedra (Fig. 1); the *c* lattice parameter would then increase with 0.043 nm, as is the case for freeze-dried MkB (Table 4). Complete occupation of the cavities and approximately one additional layer of H_2O molecules between the sheets would increase *c* by 0.16 nm as is the case for freeze-dried MkA. Possibly, some of this "intra sheet" water is expelled during freeze-drying, as a slightly smaller value for *c* is observed in freeze-dried MkA relative to suspended MkA (Table 4). The variation in lattice parameters found may thus be explained by various amounts of intercalated water. Analogous to the hematite-like materials of Dang et al. (1998), OH-groups might be structurally incorporated as well, if associated with either incorporated protons or cations, or sulfide vacancies to balance local charge deficits. This would have a similar effect on the lattice parameters as intercalated water. Obviously, the observed lattice contraction will progress, with time, toward water-free crystalline mackinawite as was shown by Kornicker (1988). If the lattice and, thus, the unit-cell expansion relative to crystalline mackinawite is caused by hydration, then the density of the solid can be estimated. The density of crystalline mackinawite is 4.5 g/cm^3. The freeze-dried FeS_{am} density calculated from the unit-cell expansions and relative contributions of MkA and MkB is 4.1 g/cm^3. This is similar to the density found by Watson et al. (2000) of 3.9 g/cm^3 for their mackinawite-greigite mixture.

The XRDP data point to at least two of the explanations for lattice expansion: lattice relaxation is supported by the negative correlation between domain size and lattice expansion, while hydration is supported by the effects of drying on lattice parameter *c* and the SSA. It is likely that several explanations apply, since disordered mackinawite originates in the reaction between a hexaquo-Fe^{2+} and either a hydrogen sulfide molecule or a bisulfide ion within the milliseconds preceding precipitation (Rickard 1995). Hydration seems to have the greatest effect on the disordered mackinawite lattice. The variation in *c* indicates that increasing amounts of water are intercalated with decreasing degree of crystallinity. Therefore, we propose that disordered mackinawite is a hydrated phase. Future work on the characterization of disordered mackinawite should include methods to test the possibility of hydration, such as weight loss measurements (DTA/DTG) or infrared spectroscopy.

TABLE 5. Summary of the characteristics of MkA and MkB end-members in precipitated and freeze-dried FeS_{am}

	MkA	MkB
Average crystallite size (nm)	2.0	5.4
Surface area (m^2/g)	~750	~300
Lattice parameters (Å)	$a = b = 4.02$ $c = 6.60$	$a = b = 3.65$ $c = 5.48$
Crystallinity (% unit-cell expansion)	54%	4%
Density (g/cm^3)	3.3	4.4

Our results show that disordered mackinawite is a nanoparticulate phase with a particle size as small as 2 nm. This conclusion is consistent with independent data from neutron scattering data (Watson et al. 2000) as well as being internally consistent. For example, the regular XRPD patterns cannot be fitted with a single set of asymmetrical peaks and the average size calculated from the MkA and MkB domains is similar to that determined by LAXRPD. However, this does raise a problem. Theoretically, the classical Braggian approach to XRPD assumes the presence of an infinite periodic lattice. Likewise, the Scherrer equation for particle size assumes that the peak broadening is entirely derived from coherence length of the structural domains. For normal particles, this is a close approximation to the effective situation. However, for nanoparticles, an infinite periodic structure cannot be assumed, although the limiting size for the breakdown of the classical approach is not well understood. Also, the Scherrer equation may not be applicable to nanoparticulate material since intra-particle disorder can also contribute significantly to the apparent coherence length. The close agreement between our particle size measurements and independent neutron scattering data suggests that, in disordered mackinawite, the contribution of intra-particle disorder is small.

It may be that the simple layer structure of mackinawite, with its dominant 0.5 nm spacing between sheets of Fe atoms, has contributed to the success of the classical approach in this particular case. For more complex structures, the classical approach might break down at larger particle sizes. It will be interesting to investigate the structure of these FeS nanoparticles using more rigorous structural analyses, when these methods become available.

Implications for the reactivity of disordered mackinawite

Disordered mackinawite is a major component of the acid volatile sulfide fraction of sediments (Berner 1970). Scavenging of trace elements by FeS_{am} is an important pathway for removal of these elements from solution in anoxic environments (Kornicker 1988; Morse and Arakaki 1993; Arakaki and Morse 1993; Morse and Luther 1999; Wharton et al. 2000). Our structural data show that disordered mackinawite is nanocrystalline and, thus, has a very high reactive surface area. It has an expanded lattice, in particular along the **c** axis, with intercalated water molecules between the tetrahedral sheets and possibly intercalated hydroxyl groups with associated protons, cations, or sulfide vacancies to balance charge. In such a flexible lattice relatively large amounts of trace elements could be taken

up, while at the reactive edge faces more trace elements could be adsorbed. The results suggest that the particle size reactivity and surface state of FeS_{am} will depend on its composition in terms of the two end-member disordered mackinawite phases. The properties of these phases, summarized in Table 5, are significantly different. This means that disordered mackinawite will react differently depending on the proportions of these two end-member forms. The proportion of the two end-member phases depends in turn on the conditions under which FeS_{am} is precipitated and its age. The main variables determining the reactivity of disordered mackinawite in ambient temperature aqueous solutions are thus pH and time.

Examples for the range in mackinawite reactivity are the variations in the solubility of FeS_{am}. With a change in the proportion of the two end-member phases, the specific surface area changes (Table 5). This will be reflected by a decrease in solubility. Moreover, if the observed lattice expansion in phase MkA is indeed caused by structurally incorporated water molecules, then the solubility of MkA will be greater than that of MkB. The solubility product is generally presented in terms of the ion activity product assuming that the activity of the ideal solid phase is unity. Deviations from ideality, as displayed by disordered mackinawite, are normally incorporated into variations in the measured solubility product. The consequence is that the solubility product of nanoparticulate, disordered mackinawite consisting of a variable mixture of end-member phases may have no meaning. The measured solubility will vary according to the conditions of formation (cf. Davison et al. 1999; Benning et al. 2000).

The experimental reactivity of FeS_{am} has been observed to vary and this, in turn, is partly explained by the age and preparation conditions of the precipitate. For example, Benning et al. (2000) showed that their freeze-dried FeS_{am} would only form pyrite in the reaction with H_2S if it was oxidized. In contrast, Rickard (1997) showed that freeze-dried FeS_{am} reacts quite readily with H_2S to form pyrite and that the stoichiometry of the reaction precluded O_2 as playing a substantive role. The present results show that freeze-dried FeS_{am} contains varying proportions of 2.0 nm and 5.4 nm particles depending on the formation conditions and the age of the FeS_{am} precipitate when freeze-dried. This will lead to different reactivities as the proportion of the highly reactive 2 nm MkA decreases, for example, with time. These observations may explain the differences in reactivity found in the experimentations described above and in the environment.

The effect of aging of FeS_{am} has been well established. After periods of days to months in aqueous solutions, crystalline mackinawite develops (Rickard 1969; Kornicker 1988). The development of crystalline mackinawite is also enhanced at elevated temperatures (Rickard 1997). Both observations are consistent with the results of this experimentation, which demonstrates that aging results in a decrease of nanoparticulate MkA and a decrease in the degree of hydration of the material. The result of these changes with time and temperature is to decrease the reactivity of FeS_{am} toward oxidation and pyrite formation. It partly explains why mackinawite can last in a metastable state for considerable periods of time in sedimentary environments (e.g., Berner 1974; Hurtgen et al. 1999) and hydrothermal and magmatic ore deposits (e.g., Kuovo et al. 1963; Evans et al. 1964; Browne and Wood 1974).

ACKNOWLEDGMENTS

P. Van Cappellen and C.H. van der Weijden (Utrecht University) and L. Charlet (Grenoble University) provided insightful discussions over the course of this study and J. Watson (Southampton University) brought to our attention the consistency of our results with the neutron scattering data. D. Rancourt (University of Ottawa) made valuable critical comments on the manuscript. The manuscript was improved by the insightful comments of J. Morse, four anonymous reviewers, and the associate editor. We thank W. Boer (NIOZ) for performing the BET measurements. This research was supported by the Netherlands Organization of Scientific Research (NWO/ALW grant 750.197.06 to M.W.), and by NERC grant NERLS200000611 to D.R. This research was conducted under the program of the Netherlands Research School of Sedimentary Geology.

REFERENCES CITED

Arakaki, T. and Morse, J.W. (1993) Coprecipitation and adsorption of Mn(II) with mackinawite (FeS) under conditions similar to those found in anoxic sediments. Geochimica et Cosmochimica Acta, 57, 9–14.

Benning, L., Wilkin, R.T., and Barnes, H.L. (2000) Reaction pathways in the Fe-S system below 100°C. Chemical Geology, 167, 25–51.

Berner, R.A. (1964) Stability fields of iron minerals in anaerobic marine sediments. Journal of Geology, 72, 826–834.

——— (1967) Diagenesis of iron sulfide in recent marine sediments. In G.H. Lauf, Ed., Estuaries (papers of a conference on estuaries, Jekyll Island 1964). American Association for the Advancement of Science, Washington, 268–272.

——— (1970) Sedimentary pyrite formation. American Journal of Science, 268, 1–23.

——— (1974) Iron sulfides in Pleistocene deep Black Sea sediments and their paleoceanographic significance. In E.T. Degens and D.A. Ross, Eds., The Black Sea: Geology, Chemistry and Biology. Max-Planck-Gesellschaft Memoir, 20, 524–531.

Brindley, G.W. (1980) Order-disorder in clay mineral structures. In G.W. Brindley and G. Brown, Eds., Crystal Structures of Clay Minerals and Their X-ray Identification, 125–195. Mineralogical Society London.

Browne, P.R.L. and Wood, C.P. (1974) Mackinawite and pyrite in a hot springs deposit, Mohaka River, New Zealand. Neues Jahrbuch für Mineralogie, Monatshefte, 10, 468–475.

Cornell, R.M. and Schwertman, U. (1996) The iron oxides, 573 p. VCH Verlag, Weinheim.

Dang, M.-Z., Rancourt, D.G., Dutrizac, J.E., Lamarche, G., and Provencher, R. (1998) Interplay of surface conditions, particle size, stoichiometry, cell parameters, and magnetism in synthetic hematite-like materials. Hyperfine Interactions, 117, 271–319.

Dixit, S. and Van Cappellen, P. (2002) Surface chemistry and reactivity of biogenic silica. Geochimica et Cosmochimica Acta, 66, 2559–2568.

Dzombak, D.A. and Morel, F.M.M. (1990) Surface Complexation Modelling, Hydrous Ferric Oxide. Wiley, New York.

Echt, O., Reyes Flotte, A., Knapp, M., Sattler, K., and Recknagel, E. (1982) Magic numbers in the mass spectra of Xe, $C_2F_4Cl_2$ and SF_6 clusters. Berichte der Bunse-Gesellschaft für Physikalische Chemie, 86, 860–865.

Evans, Jr., H.T., Milton, C., Chao, E.C.T., Adler, I., Mead, C., Ingram, B., and Berner, R.A. (1964). Vallerite and the new iron sulfide, mackinawite. USGS Professional Paper 475-D, 64–69.

Hurtgen, M.T., Lyons, T.W., Ingall, E.D., and Cruse, A.M. (1999) Anomalous enrichments of iron monosulfide in euxinic marine sediments and the role of H_2S in iron sulfide transformations: examples from Effingham Inlet, Orca Basin, and the Black Sea. American Journal of Science, 299, 556–588.

Kornicker, W.A. (1988) Interactions of divalent cations with pyrite and mackinawite in seawater and sodium-chloride solutions. Ph.D. thesis. Texas A&M University.

Kuovo, O., Vuorelainen, Y., and Long, J.V.P. (1963) A tetragonal iron sulfide. American Mineralogist, 48, 511–524.

Lennie, A.R. and Vaughan, D.J. (1996) Spectroscopic studies of iron sulfide formation and phase relations at low temperatures. Mineral Spectroscopy, 5, 117–131.

Lennie, A.R., Redfern, S.A.T., Schofield, P.F., and Vaughan, D.J. (1995) Synthesis and Rietveld crystal structure refinement of mackinawite, tetragonal FeS. Mineralogical Magazine, 59, 677–683

Luther, III, G.W., Theberge, S.M., and Rickard, D.T. (1999) Evidence for aqueous clusters as intermediates during zinc sulfide formation. Geochimica et Cosmochimica Acta, 63, 3159–3169.

Luther, III, G.W., Rozan, T.F., Taillefert, M., Nuzzio, D.B., Di Meo, C., Shank, T.M., Lutz, R.A., and Cary, S.C. (2001) Chemical speciation drives hydrothermal vent ecology. Nature, 410, 813–816.

McEwan, D.M.C., Ruiz, A.A., and Brown, G. (1961) Interstratified clay minerals.

In G.W. Brindley and G. Brown, Eds., Crystal Structures of Clay Minerals and Their X-ray Identification. Mineralogical Society London, 393–445.
Morse, J.W. and Arakaki, T. (1993) Adsorption and coprecipitation of divalent metals with mackinawite (FeS). Geochimica et Cosmochimica Acta, 57, 3635–3640.
Morse, J.W. and Luther, III, G.W. (1999) Chemical influences on trace metal-sulfide interactions in anoxic sediments. Geochimica et Cosmochimica Acta, 63, 3373–3378.
Morse, J.W., Millero, F.J., Cornwell, J.C., and Rickard, D. (1987) The chemistry of the hydrogen sulfide and iron sulfide systems in natural waters. Earth-Science Reviews, 24, 1–42.
Mullet, M., Boursiquot, S., Abdelmoula, M., Génin, J.-M., and Ehrhardt, J.-J. (2002) Surface chemistry and structural properties of mackinawite prepared by reaction of sulfide ions with metallic iron. Geochimica et Cosmochimica Acta, 66, 829–836.
Murowchick, J.B. and Rickard, D.T. (1997) Structural changes during ripening of synthetic mackinawite formed by corrosion of alpha-iron. Abstracts with Programs, Geological Society of America, 29, 402.
Parfitt, R.L., Van der Gaast, S.J., and Childs, C.W. (1992) A structural model for natural siliceous ferrihydrite. Clays and Clay Minerals, 40, 675–681.
Rickard, D.T. (1968) The geological and microbiological formation of iron sulfides. Ph.D. thesis, London University.
——— (1969) The chemistry of iron sulphide formation at low temperatures. Stockholm Contributions in Geology, 20, 67–95.
——— (1975) Kinetics and mechanism of pyrite formation at low temperatures. American Journal of Science, 275, 636–652.
——— (1995) Kinetics of FeS precipitation: Part 1. Competing reaction mechanisms. Geochimica et Cosmochimica Acta, 59, 4367–4379.
——— (1997) Kinetics of pyrite formation by the H_2S oxidation of iron(II) monosulfide in aqueous solutions between 25 and 125°C: The rate equation. Geochimica et Cosmochimica Acta, 61, 115–134.
Rickard, D. and Luther, III, G.W. (1997) Kinetics of pyrite formation by the H_2S oxidation of iron(II) monosulfide in aqueous solutions between 25 and 125°C: The mechanism. Geochimica et Cosmochimica Acta, 61, 135–147.
Rickard, D., Schoonen, M.A.A., and Luther, III, G.W. (1995). The chemistry of iron sulfides in sedimentary environments. In M.A. Vairavamurthy and M.A.A. Schoonen, Eds., Geochemical transformations of sedimentary sulfur. ACS symposium series 612, 168–193.
Rickard, D., Oldroyd, A., and Cramp, A. (1999) Voltammetric evidence for soluble FeS complexes in anoxic estuarine muds. Estuaries, 22, 693–701.
Spadini, L., Bott, M., Wehrli, B., and Manceau, A. (2003) Analysis of the major Fe bearing phases in recent lake sediments by EXAFS spectroscopy, in press.
Taylor, L.A. and Finger, L.W. (1970) Structural refinement and composition of mackinawite. Carnegie Instution of Washington, Geophysical Laboratory Annual Report, 69, 318–322.
Taylor, P., Rummery, T.E., and Owen, D.G. (1979) On the conversion of mackinawite and greigite. Journal of Inorganic and Nuclear Chemistry, 41, 595–596.
Theberge, S.M. and Luther, III G.W. (1997) Determination of the electrochemical properties of a soluble aqueous FeS species present in sulfidic solutions. Aquatic Geochemistry, 3, 191–211.
Van der Gaast, S.J., Wada, K., Wada, S.I., and Kakuto, Y. (1985) Small-angle X-ray powder diffraction, morphology, and structure of allophane and imogolite. Clays and Clay Minerals, 33, 237–243.
Van der Gaast, S.J., Mizota, C., and Jansen, J.H.F. (1986) Curved smectite in soils from volcanic ash in Kenya and Tanzania: a low-angle X-ray powder diffraction study. Clays and Clay Minerals, 34, 665–671.
Vaughan, D.J. (1970) Nickelian mackinawite from Vlakfontein: a reply. American Mineralogist, 55, 1807–1808.
Vaughan, D.J. and Craig, J.R. (1978) Mineral chemistry of metal sulfides, 493 p. Cambridge University Press, Cambridge.
Watson, J.H.P., Cressey, B.A., Roberts, A.P., Ellwood, D.C., Charnock, J.M., and Soper, A.K. (2000) Structural and magnetic studies on heavy-metal-adsorbing iron sulphide nanoparticles produced by sulphate-reducing bacteria. Journal of Magnetism and Magnetic Materials, 214, 13–30.
Waychunas, G.A. (2001) Structure, aggregation and characterization of nanoparticles. In J.F. Banfield and A. Navrotsky, Eds., Nanoparticles and the environment, vol. 44, 105–166. Reviews in Mineralogy and Geochemistry, Mineralogical Society of America, Washington, D.C.
Wharton, M.J., Atkins, B., Charnock, J.M., Livens, F.R., Pattrick, R.A.D., and Collison, D. (2000) An X-ray absorption spectroscopy study of the coprecipitation of Tc and Re with mackinawite (FeS). Applied Geochemistry, 15, 347–354.
Widler, A.M. and Seward, T. M. (2002) The adsorption of gold(I) hydrosulphide complexes by iron sulphide surfaces. Geochimica et Cosmochimica Acta, 66, 383–402.

MANUSCRIPT RECEIVED OCTOBER 1, 2002
MANUSCRIPT ACCEPTED MAY 28, 2003
MANUSCRIPT HANDLED BY UDO BECKER